Development and Characterization of $Ti_{50}Ni_{25}Pd_{25}$ Ternary Shape Memory Alloy through Powder Metallurgy Route

Abid Hussain[1], Afzal Khan[1], M. Imran Khan[2], Saif ur Rehman[3]

1. University of Engineering and Technology Peshawar, Pakistan,
2. Ghulam Ishaq Khan (GIK) Institute of Engineering and Science and Technology, Topi District Swabi, Khyber Pakhtunkhwa 23640, Pakistan
3. Institute of Industrial Control System, Rawalpindi, Pakistan

Abstract-This study gives a thorough analysis into the use of powder metallurgy to create a TiNiPd ternary shape memory alloy (SMA). Focusing on comparing alloys created using the argon-arc melting process, the study examines the effects of compacting pressure and copper concentration on transition temperature and thermal hysteresis. A thorough microstructural analysis was performed to look at how solution treatment, annealing, and ageing affected the phase transformation temperatures and shape memory properties. The outcomes showed that the alloy microstructure was altered by the annealing and ageing processes, resulting in the production of stable high-temperature precipitates. Notably, ageing and solution treatment increased hardness values and decreased porosity %. These results highlight the critical importance of particular elemental substitutions and processing factors in modifying the TiNiPd SMA's characteristics and expanding the range of applications for which it can be used. The knowledge gathered from this study's insights is useful for building and optimising novel ternary shape memory alloys with improved performance properties. It also advances the field of shape memory alloys.

Keywords: TiNiPd ternary shape memory alloy, DSC, XRD, SEM, EDX, Brinell Hardness Test, Heat Treatment.

1. Introduction:

Shape Memory Alloys (SMAs) have drawn a lot of attention due to their outstanding pseudoelasticity and amazing shape memory effect in a variety of sectors, including engineering and medical. [1]. Shape memory alloys (SMAs) are a unique class of metallic materials that display an intriguing characteristic known as the shape memory effect (SME). The distinctive property of SMAs that allows them to return to their original shape after deformation when heated over a certain temperature defines this SME. This behavior is caused by the reversible phase transformation in SMAs between austenite and martensite. Notably, the return of the original shape is made easier by the transformation from martensite to austenite following heating. Different varieties of SMAs can exhibit either one-way or two-way SME depending on their unique composition and intended applications. [2].

The United States Naval Ordinance Laboratory created the first shape memory alloy for the Ni-Ti system, known as "NiTiNOL." The extraordinary elasticity and the temperatures at which the austenitic and martensitic transitions take place of Ni-Ti shape memory alloys have both been the subject of extensive research into their properties and applications [3]. The thermoresponsive properties of these alloys have led to their classification as smart materials [4]. Shape memory alloys and piezoelectric materials fall under this category. The transition of these alloys from the low-temperature phase (martensite) to the high-temperature phase (austenite) is one of their key characteristics) [5].

The shape memory alloy (SMA) nickel titanium (NiTi) is often used, but because to its poor workability and casting-related difficulties, there is interest in investigating powder metallurgy (PM) techniques for near-net shape processing. However, there is still a big obstacle to getting PM-produced NiTi SMA alloys with cast alloy-like characteristics. In this context, the recoverable strain, a fundamental SMA quality measure widely addressed in literature, is significant. [6]. Using the pressure-enhanced sintering method known as Health Information Provider Services (HIPS), powders are packed into gas-tight welded cans under vacuum before being subjected to pressure. Hot isostatic pressing (HIPS) of prealloyed powders produces the most uniform and virtually theoretically dense samples. [7] Kato et al. According to the findings, these samples exhibited 12% fracture strains and 6% martensite plateau strains. Despite having brittle fracture at first, the specimens' recoverable strain may be on par with cast alloys. Similar results were found in Johansen's investigation, where a NiTi alloy supplemented with TiC particles managed a 4% strain recovery and a 10% total strain under HIP circumstances.

The transition temperatures (TTs) of NiTiHf remain largely steady at lower concentrations of Hf, according to both experimental evidence and first-principle calculations. However, a considerable Hf concentration (over 15%) causes a huge rise in the TTs, which can exceed 350 °C. [8]. Furthermore, compared to NiTi, NiTiHf alloys display extraordinary a lack of slipping, resulting in larger transformation strains in both tension and compression.[9]. It is crucial to emphasise that, in contrast to transformation temperatures (TTs), a NiTiHf alloy's transformation strains even be impacted by slight modification to the Hf fraction. [10]. Understanding the characteristics of NiTiHf has been the focus of intensive research over the last ten years. It has been discovered that the alloying composition of NiTiHf has a significant impact on its thermomechanical properties. The thermomechanical characteristics of NiTiHf are also influenced by a number of other variables, for instance, heating, precipitation, grain size, and the type of load (tension vs. compression). To further understand its characteristics, extensive research is therefore desperately needed. It is important to note that there have only been a few compositions studied for NiTiHf. [11]. As a result, there hasn't been a thorough investigation into how different variables affect how these High-Temperature Shape Memory Alloys (HTSMAs) behave. Given the challenges and complexity involved in synthesising different compositions of these alloys, computational simulations, such as atomistic approaches, have proven to be highly advantageous in estimating and predicting the material properties of new NiTiHf alloy compositions in a time- and cost-efficient manner. Molecular dynamics (MD) stands out as one of the best methods for extensively examining the microstructural factors that control material behaviour among various atomistic modelling techniques. Interatomic potentials, however, which are the MD constitutive equations and specify the forces and interactions between atoms, are extremely important to the precision of MD simulations. Therefore, it is essential to create reliable interatomic potentials in order to guarantee the accuracy of MD simulations. [12].

The Schrödinger equation's description of the actual quantum mechanical interactions is based on analytical functional forms known as interatomic potentials, which are mathematical approximations of these functional forms. [13]. If an interatomic potential accurately mimics the mechanical characteristics of an alloy with diverse compositions, it can be considered a trustworthy instrument. [14]. To look into a variety of atomic-scale materials science issues, there are numerous classes of parametric potentials. [15]. The many-body potential, which depends on the local electron density, stands out as one of the most precise types of interatomic potential intended for metals. [16]. The development of various kinds of many-body potentials has received significant attention, leading to the development of techniques like the Finnis-Sinclair (FS) potential. [17], embedded-atom method (EAM) [18], modified embedded atom method (MEAM). The approximate second-moment of the tight-binding potential is one of many many-body potentials that have undergone extensive research. (TB-SMA) [19].

The creation and characterisation of the Ti50Ni25Pd25 alloy are the main topics of the current study. After that, the outcomes are contrasted with those of the TiNiHf alloy.

2. Experimental Procedures

Titanium, Nickel, and Palladium micro powders with a purity of more than 99% were used in this investigation. As shown in Figures 1, 2, and 3, a Ti50Ni25Pd25 ternary alloy was created, and its properties were examined using SEM, EDX, and XRD methods. While the Ti, Ni, and Cu powders came from FS Corporation in Lahore, Pakistan, and were 99.3% pure, the Pd powders were from YURUI (SHANGHAI) Chemical Co., Limited in China. Using image J and Fiji software, the purity and particle size of the powders are displayed in Table 1.

Through two hours of ball milling, the powders were combined according to their atomic percentages. The combined powders were then sintered at 950°C for ten minutes in a vacuum furnace under regulated air conditions, then cold compacted at 800 MPa using a hydraulic press. The alloys were then treated with a solution at 900°C for the same amount of time after being homogenised at 1000°C for two hours in a vacuum furnace.

The remaining alloys were annealed at 700°C, slowly cooled in a furnace, then aged for six hours at 800°C after being cut into one-millimeter-thick sections. Table 2 gives details on each of the 12 samples that were used in the experiment.

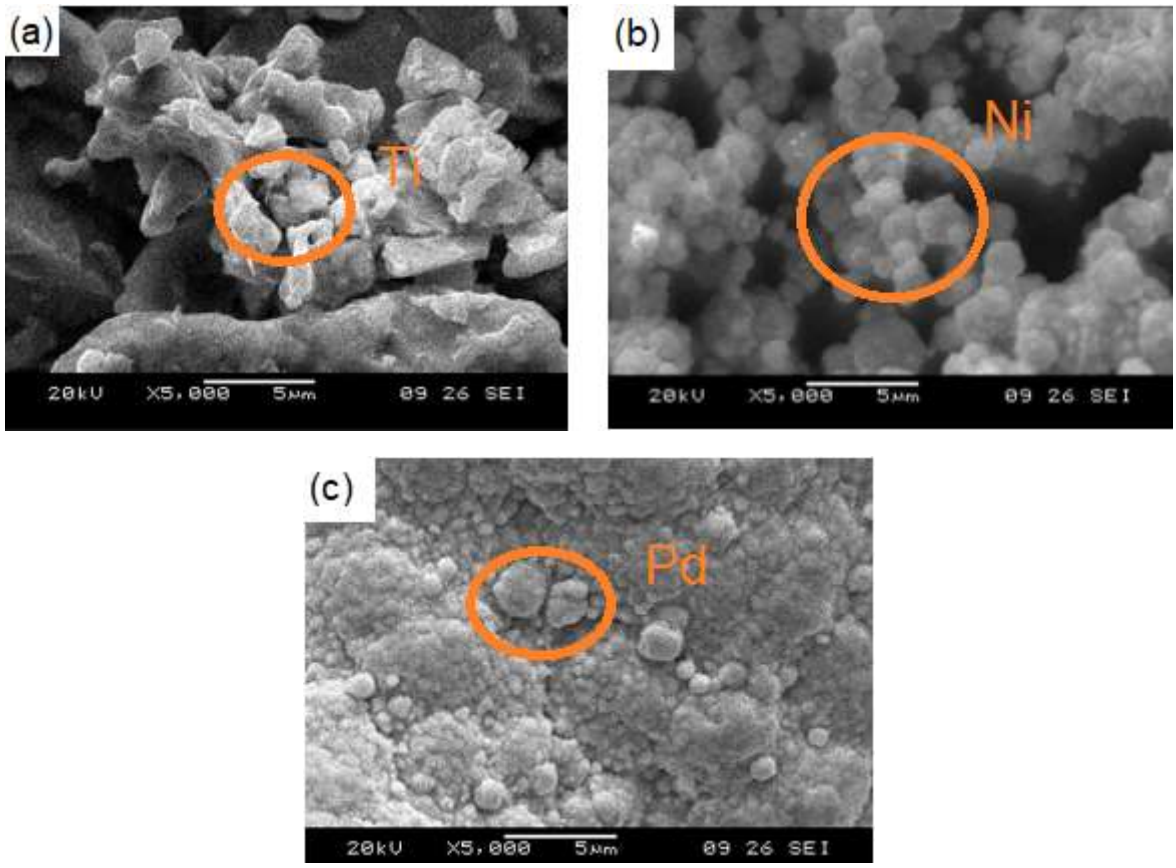

Fig. 1 SEM images of (a) Ti, (b) Ni and (c) Pd powders

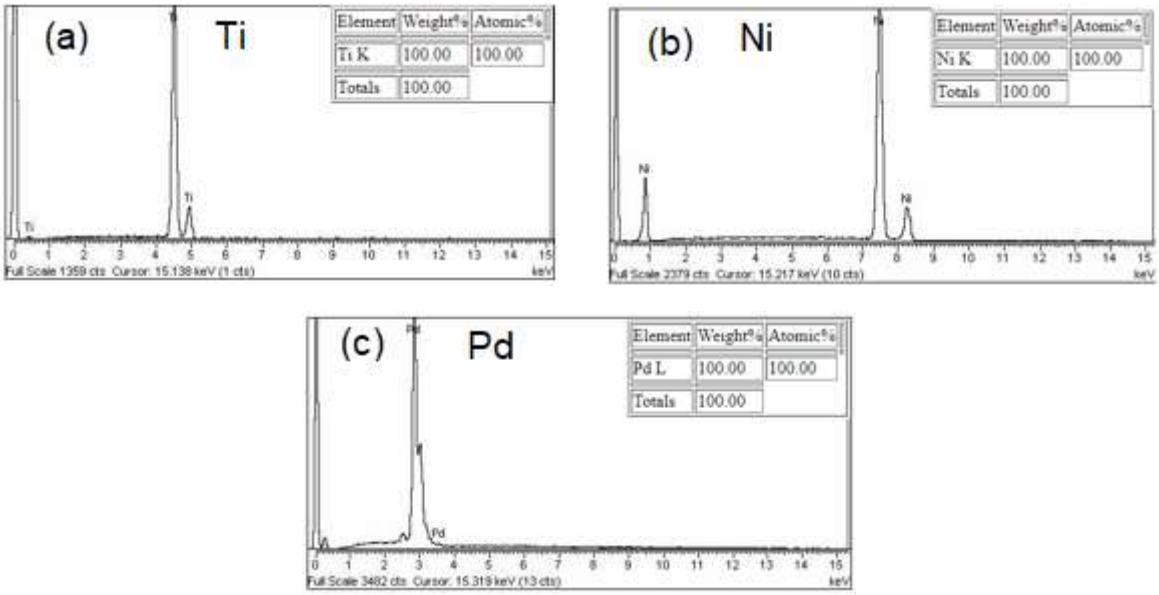

Fig. 2 EDX of (a) Ti, (b) Ni and (c) Pd Powders

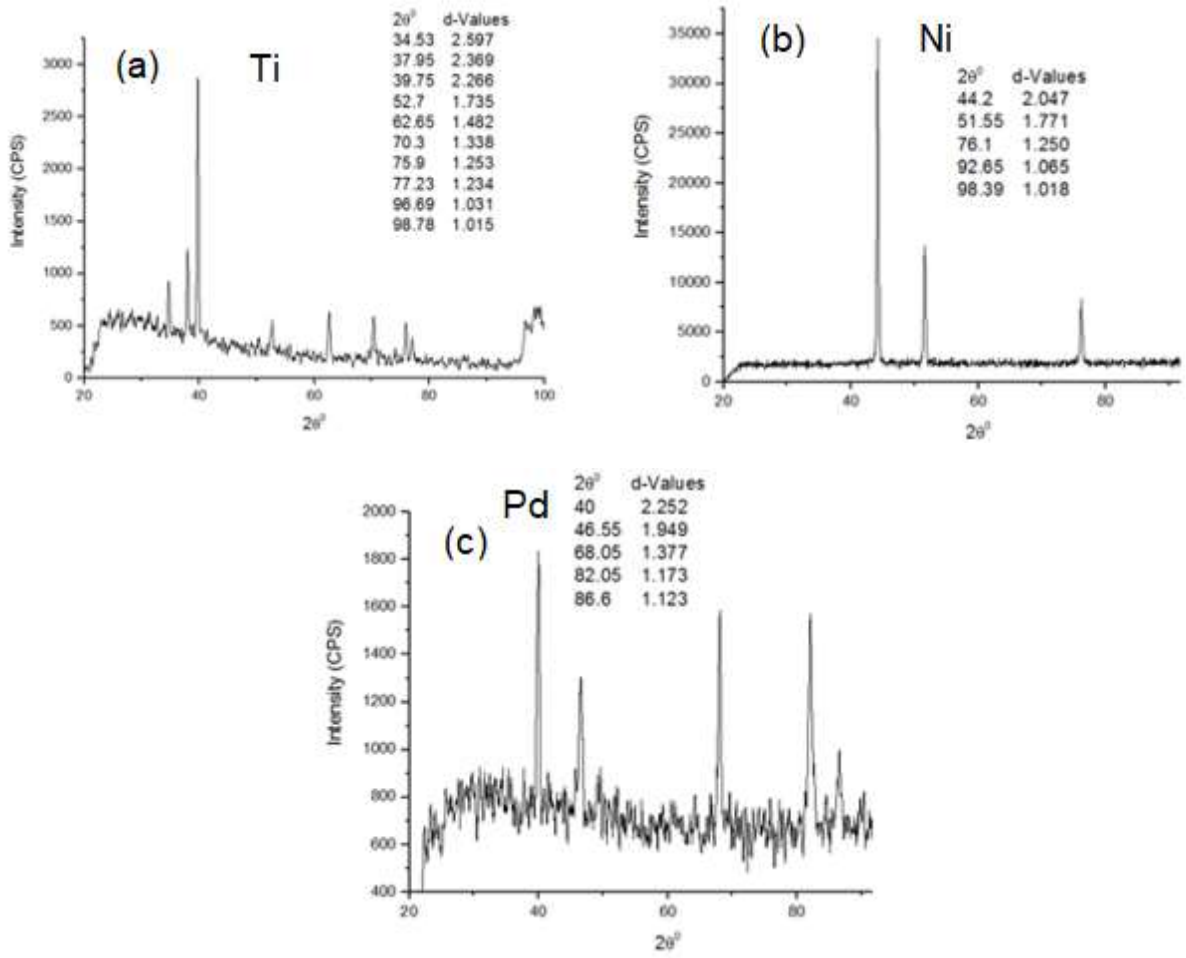

Fig. 3 XRD of (a) Ti, (b) Ni and (c) Pd Powder at room temperature

Table 1: Purity (%) and Particle Size (µm) of Powder used

Metal (Powder)	Purity (wt%)	Particle Size (µm)
Ti	99	35
Ni	99	2
Pd	99.1	51

Scanning electron microscopy (SEM) pictures of Ti, Ni, Cu, and Pd powders are shown in Figure 1(a), (b), (c), and (d), and the corresponding particle sizes are determined using Image J and Fiji software, with the values given in Table 1. Red circles are used to emphasise the particles.

The Energy Dispersive X-Ray Analysis (EDX) of these powders is shown in Figure 2 (a, b, c, and d), demonstrating their purity.

Additionally, TiNiPdCu powders' X-Ray Diffraction (XRD) patterns are shown in Figure 3 (a, b, c, and d), confirming their crystalline structure. All samples' porosity was calculated using their densities. [5].

percentage porosity = $\left[1 - \left(\frac{p_r}{p_0}\right)\right] * 100$ ---------- (1)

p_r, shows the actual density of the alloy and can be found by dividing their weight by volume. p_0, shows theoretical density of alloy and calculated as

$P_0 = \left[\left(P_0^{Ni}\right) * at\%Ni\right] + \left[\left(P_0^{Ti}\right) * at\%Ti\right] + \left[\left[\left(P_0^{Cu}\right) * at\%Cu\right] + \left[\left[\left(P_0^{Pd}\right) * at\%Pd\right]\right.\right.$ ---------- (2)

Where P_0^{Ni}, P_0^{Ti}, P_0^{Cu} and P_0^{Pd} shows theoretical densities of Ni, Ti, Cu and Pd respectively.

The Brinell Hardness Tester was utilized to conduct the hardness test on the alloy.

3. Results and Discussions

3.1.Transformation Temperatures

The Ti50Ni25Pd25 ternary shape memory alloy underwent differential scanning calorimetry (DSC) study, which involved heating and cooling cycles as shown in Figure 4. The alloy's Ms, Mf, As, and Af (martensitic start temperature, austenitic start temperature, and austenitic finish temperature) were all quantified using this analysis. However, the homogenised sample DSC analysis revealed that. As seen in Fig. 4, it was discovered that the transition temperatures could not be calculated. The transition temperatures for alloys that have been aged, solution-treated, and annealed are listed in Table 2.

The results showed that the transition temperatures in the annealed condition were greater than those in the solution treatment and ageing conditions. Additionally, thermal hysteresis was minimized in the annealed alloys compared to the solution-treated and aged alloys.

Table 2: Transformation temperatures for $Ti_{50}Ni_{25}Pd_{25}$ solution treated alloy

Alloy	Transformation Temperature (^{0}C)				Thermal hysteresis
	Ms	Mf	As	Af	Af - Ms
Annealing	168	162	171	188	20
Solution Treatment	152	145	175	182	30
Aging	158	148	178	183	25

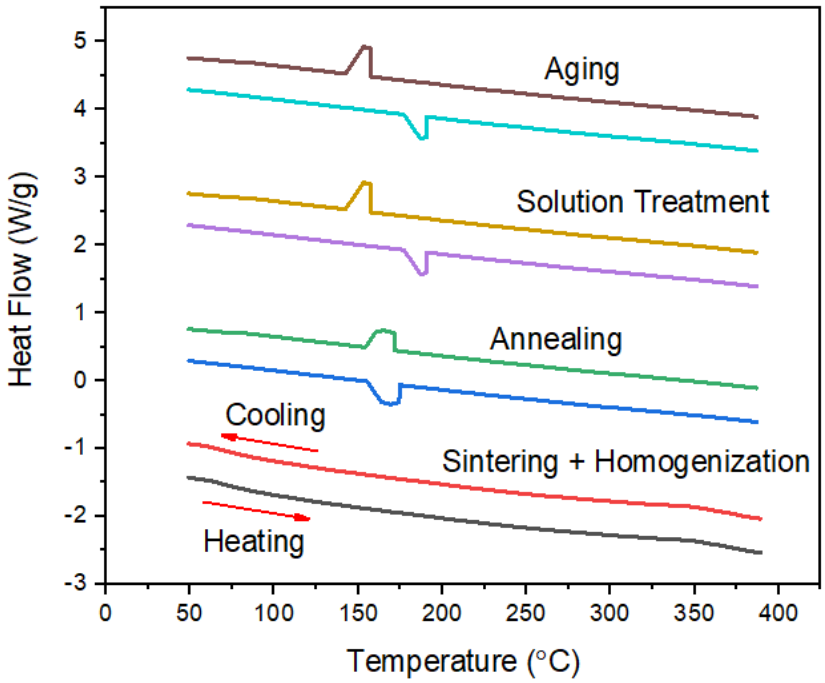

Fig. 4 DSC curves of (a) sintered and homogenized (b) homogenized and solution treated (c) solution treated and annealed (d) solution treated and aged alloy

3.2. Brinell Hardness Test

Table 3 displays the results of the Brinell hardness test. Figure 5 shows that the hardness value increases during solution treatment and ageing while decreasing during annealing. This trend can be traced to the material being more ductile during annealing, which then softened it and decreased its hardness. On the other hand, the material gets more brittle with age and solution treatment, increasing hardness.

Table 3 Brinell Hardness Test of 4 alloys

Sample No.	Composition	Heat Treatment	Brinell Hardness (HBW)
1	$Ti_{50}Ni_{25}Pd_{25}$	Sintered & Homogenized	95.7
2	$Ti_{50}Ni_{25}Pd_{25}$	Homogenized & Solution Treated	459.1
3	$Ti_{50}Ni_{25}Pd_{25}$	Solution Treated & Annealed	180.8
4	$Ti_{50}Ni_{25}Pd_{25}$	Solution Treated & Aged	466.5

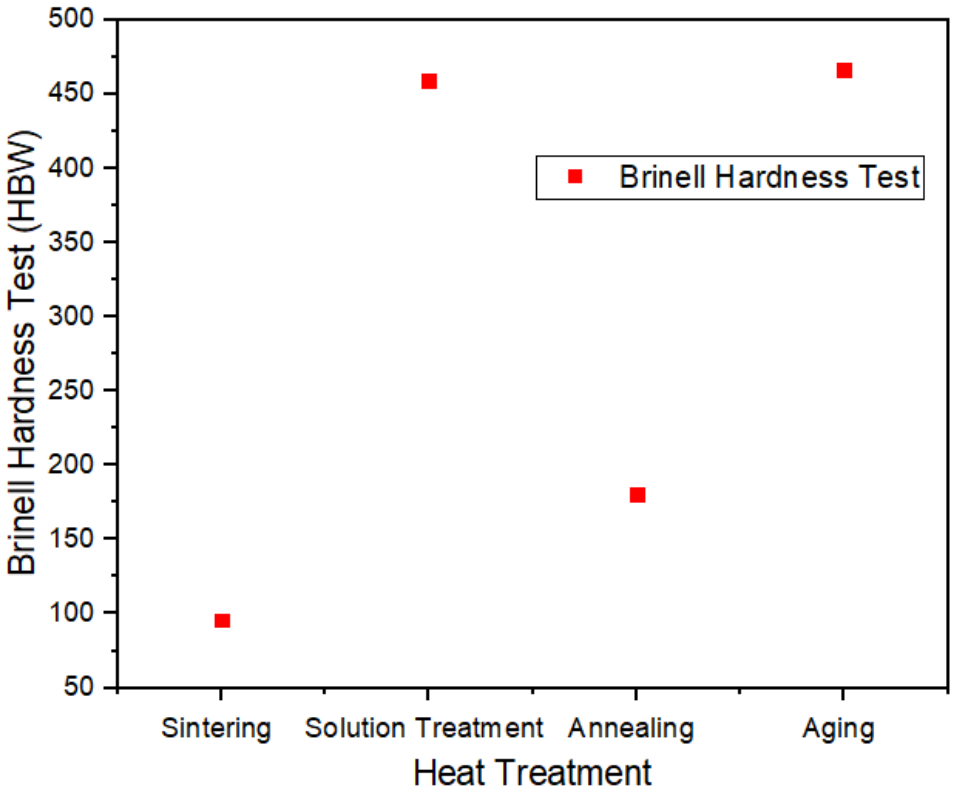

Fig. 5 Effect of hardness of $Ti_{50}Ni_{25}Pd_{25}$ SMA on homogenization, solution treatment, annealing and aging

3.3.Porosity

The % porosity values of four samples are shown in Table 4. Figure 6's data shows how the percentage of porosity is reduced during the annealing process in comparison to solution treatment and ageing. This observation is consistent with earlier studies in the literature, which show that raising the compacting pressure causes the percentage of porosity to decrease. For instance, a study showed that the percentage of porosity reduced as the compacting pressure was increased from 300 MPa to 800 MPa. [3]. The compacting pressure for this investigation was set at 800 MPa.

Table 4: % Porosity of alloys

Sample No.	Composition	Heat Treatment	Porosity (%)
1	$Ti_{50}Ni_{25}Pd_{25}$	Sintered & Homogenized	13.4
2	$Ti_{50}Ni_{25}Pd_{25}$	Homogenized & Solution Treated	13.89
3	$Ti_{50}Ni_{25}Pd_{25}$	Solution Treated & Annealed	13.01
4	$Ti_{50}Ni_{25}Pd_{25}$	Solution Treated & Aged	13.95

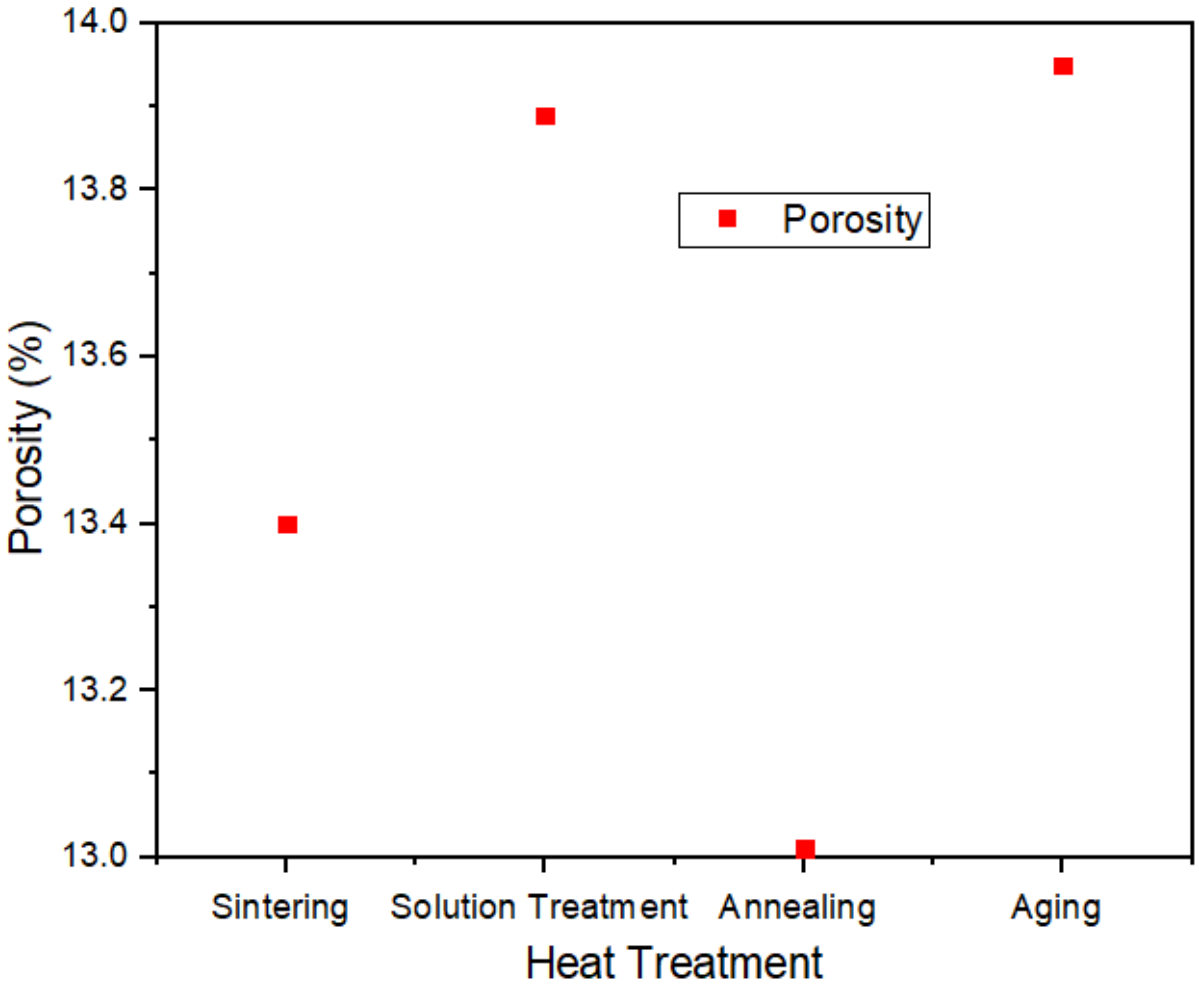

Fig. 6 Percentage porosity of $Ti_{50}Ni_{25}Pd_{25}$ SMA vs sintering, solution treatment, annealing and aging

3.4.Shape Memory Effect

A sample with the following dimensions: 14 mm 2 mm 1 mm was created and heated in a solution for one hour at 850°C before being quenched in water at room temperature. Differential scanning calorimetry (DSC) analysis was used to determine the martensitic initiation temperature. The sample was then bent at an angle of 900 while submerged in ice water, causing a 6.66% deformation. The sample was then given 40 seconds to recover in boiling water. The reference offered in this article provides a list of the expressions used in this inquiry. [20] The recovery strains of the Ti50Ni25Pd25 alloy are shown in Table 5, and they were computed using the techniques used to compute deformation and recovery strains. The samples were then distorted in frozen water at a strain rate of 6.66%.

Table 5: Deformation and Recovery strain of solution treated $Ti_{50}Ni_{25}Pd_{25}$ alloy

Alloy	Composition	Deformation Ɛ(%)	Recovery Strain ɳ(%)
1	$Ti_{50}Ni_{25}Pd_{25}$	6.66	90

3.5.Microstructural Analysis

Shape memory alloys (SMA) that have been homogenised, solution-treated, annealed, and aged are shown in Figures 7(a), (b), (c), and (d), respectively. The examination of these images indicates the existence of prominent, micron-sized, black precipitates that are readily discernible. The white precipitates, in comparison, are less prominent and are in the nano size range. Using Fiji software, image analysis was done to establish the average size of both white and black precipitates. The photos also show several pores with a size of a few microns.

Notably, compared to the annealed and aged alloys, the precipitates in the solution-treated alloys are more visible. As can be seen from Figure 10, compared to the aged and solution-treated alloys, the annealed alloy had the least porosity. Additionally, the study found that when the Cu content rises, the size of the precipitates grows while the pore size reduces, improving the alloy's mechanical qualities.

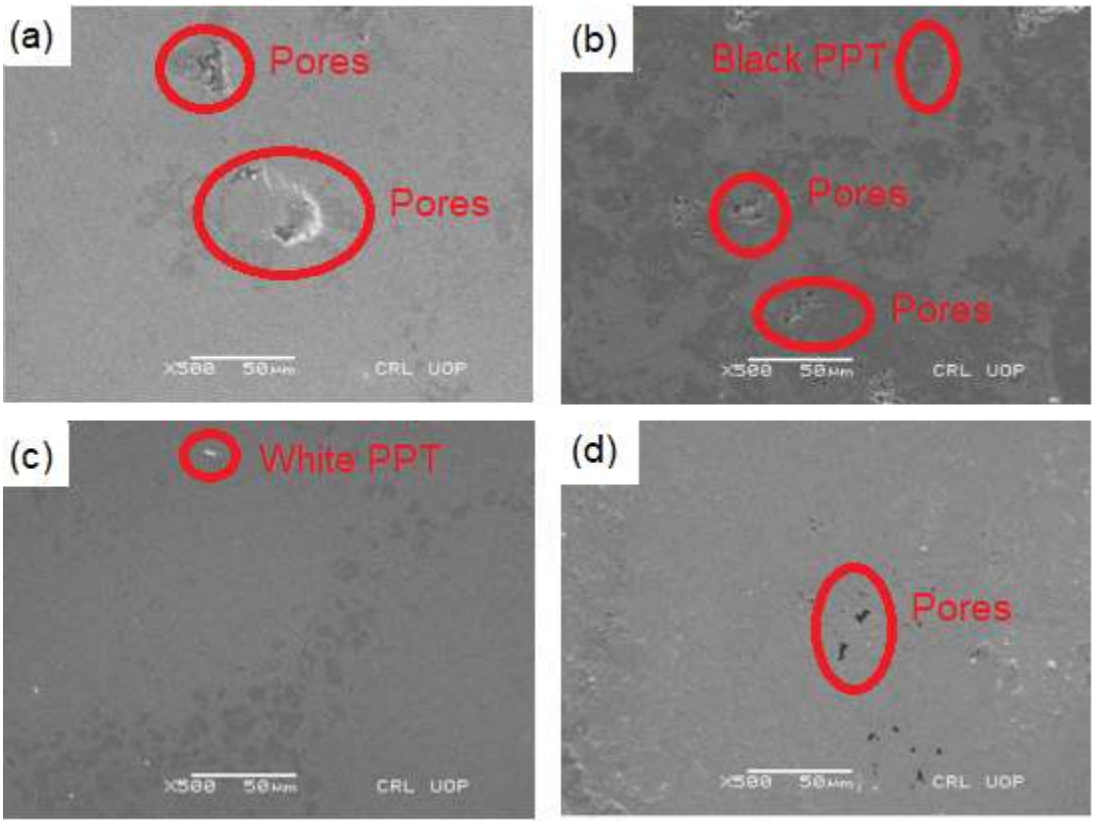

Fig. 7 SEM images of (a) Homogenized, (b) Solution Treated, (c) Annealed and (d) Aged SMA

The XRD pattern of Ti50Ni25Pd25 alloys is shown in Figure 7 under various conditions, including homogenised, solution treated, annealed, and aged. Only the martensite phase may be seen in the homogenised, solution treated, and annealed states. The SEM photos, on the other hand, show that in the aged alloy, both black and white precipitates become apparent.

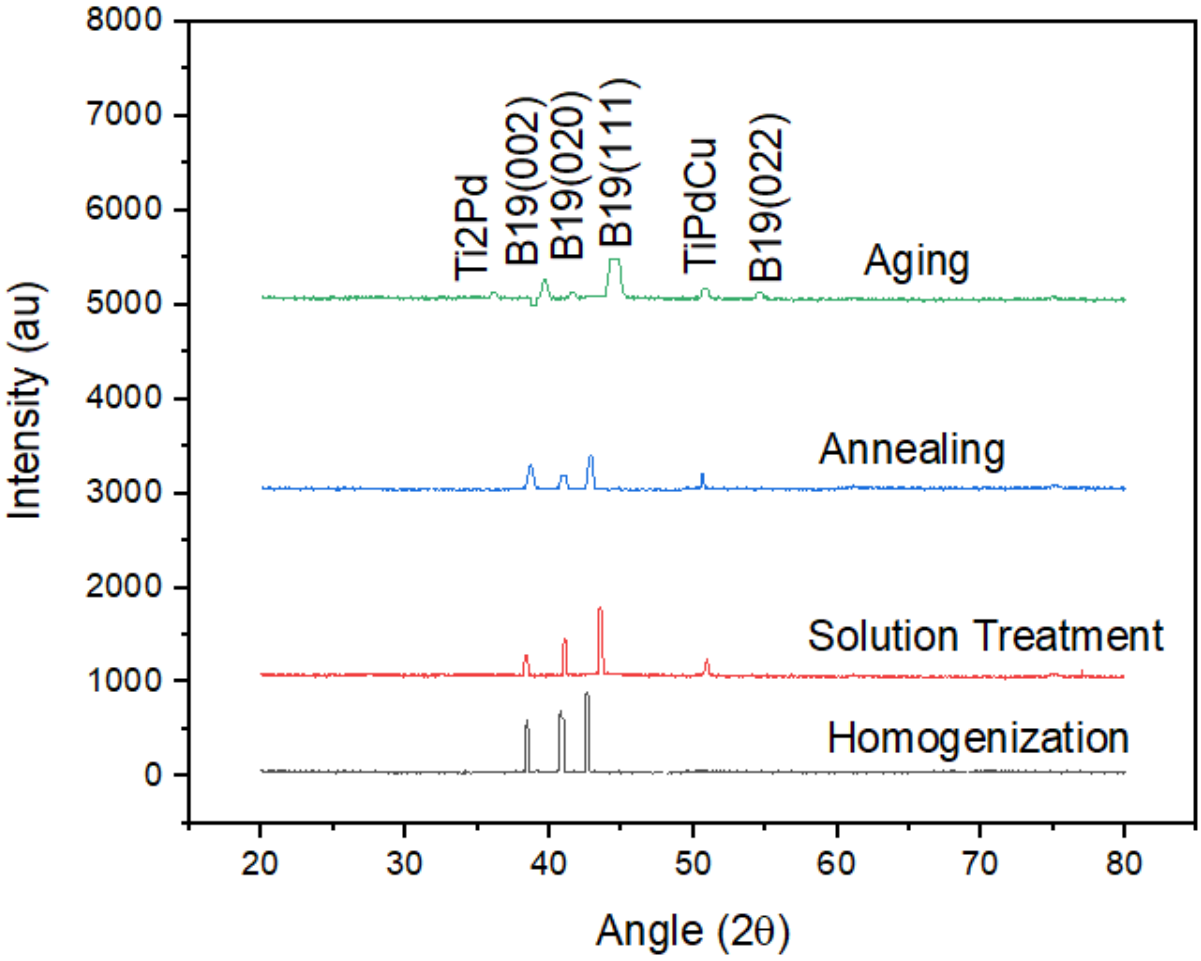

Fig. 8 XRD profile of homogenized, solution treated, annealed and aged samples

4. Conclusion

Different heat treatment techniques result in a noticeable rise in the transition temperature (Ms). Both martensitic and austenitic phases are present, according to the differential scanning calorimetry (DSC) data, which also show a significant rise in transformation temperatures and a decline in thermal hysteresis. In comparison to annealing and ageing treatments, the hardness value dramatically rises during the solution treatment process.

When compared to the solution treatment and ageing procedures, the annealing procedure also helps to lower the percentage of porosity. The existence of black and white precipitates, which are in charge of enhancing the alloy's mechanical properties, is confirmed by SEM and XRD examination.

These alloys are high-temperature shape memory alloys and can be used in high-temperature sensors and actuators since their martensitic transition temperature is greater than 100°C. It is noteworthy that the alloy's transformation temperature is higher than that of TiNiHf ternary alloys and that its thermal hysteresis is lower.

References

[1] M. Khan, A. N. Khan, S. H. I. Jaffery, L. Ali, and A. Mubashar, "Improvement in the Mechanical Properties of High Temperature Shape Memory Alloy (Ti 50 Ni 25 Pd 25) by Copper Addition," *Adv. Mater. Sci. Eng.*, vol. 2015, 2015.

[2] A. Khan, "Characterization and Application of Shape Memory Alloy Wires for Micro and Meso

Positioning Systems." The George Washington University, 2008.

[3] R. Purohit, K. K. Patel, G. K. Gupta, and R. S. Rana, "Development of Ni-Ti Shape Memory Alloys through Novel Powder Metallurgy Route and Effect of Rolling on their properties," *Mater. Today Proc.*, vol. 4, no. 4, pp. 5330–5335, 2017.

[4] L. Krone, E. Schüller, M. Bram, O. Hamed, H.-P. Buchkremer, and D. Stöver, "Mechanical behaviour of NiTi parts prepared by powder metallurgical methods," *Mater. Sci. Eng. A*, vol. 378, no. 1–2, pp. 185–190, 2004.

[5] A. S. Jabur, J. T. Al-Haidary, and E. S. Al-Hasani, "Characterization of Ni–Ti shape memory alloys prepared by powder metallurgy," *J. Alloys Compd.*, vol. 578, pp. 136–142, 2013.

[6] M. Bram, A. Ahmad-Khanlou, A. Heckmann, B. Fuchs, H. P. Buchkremer, and D. Stöver, "Powder metallurgical fabrication processes for NiTi shape memory alloy parts," *Mater. Sci. Eng. A*, vol. 337, no. 1–2, pp. 254–263, 2002.

[7] H. Kato, J. Dutkiewicz, and S. Miura, "Superelasticity and shape memory effect in Cu-23at.% Al-7at.% Mn alloy single crystals," *Acta Metall. Mater.*, vol. 42, no. 4, pp. 1359–1365, 1994.

[8] B.-J. Lee, "A modified embedded-atom method interatomic potential for the Fe–C system," *Acta Mater.*, vol. 54, no. 3, pp. 701–711, 2006.

[9] B.-J. Lee, W.-S. Ko, H.-K. Kim, and E.-H. Kim, "The modified embedded-atom method interatomic potentials and recent progress in atomistic simulations," *Calphad*, vol. 34, no. 4, pp. 510–522, 2010.

[10] J. Wolff, M. Franz, J.-E. Kluin, and D. Schmid, "Vacancy formation in nickel and α-nickel-carbon alloy," *Acta Mater.*, vol. 45, no. 11, pp. 4759–4764, 1997.

[11] G. S. Bigelow, A. Garg, S. A. Padula Ii, D. J. Gaydosh, and R. D. Noebe, "Load-biased shape-memory and superelastic properties of a precipitation strengthened high-temperature Ni50. 3Ti29. 7Hf20 alloy," *Scr. Mater.*, vol. 64, no. 8, pp. 725–728, 2011.

[12] A. P. Thompson *et al.*, "LAMMPS-a flexible simulation tool for particle-based materials modeling at the atomic, meso, and continuum scales," *Comput. Phys. Commun.*, vol. 271, p. 108171, 2022.

[13] P. Hirel, "Atomsk: A tool for manipulating and converting atomic data files," *Comput. Phys. Commun.*, vol. 197, pp. 212–219, 2015.

[14] L. Yahia, *Shape memory implants*. Springer Science & Business Media, 2012.

[15] M. Es-Souni, M. Es-Souni, and H. Fischer-Brandies, "Assessing the biocompatibility of NiTi shape memory alloys used for medical applications," *Anal. Bioanal. Chem.*, vol. 381, pp. 557–567, 2005.

[16] J. Ma, I. Karaman, and R. D. Noebe, "High temperature shape memory alloys," *Int. Mater. Rev.*, vol. 55, no. 5, pp. 257–315, 2010.

[17] G. S. Firstov, J. Van Humbeeck, and Y. N. Koval, "High temperature shape memory alloys problems and prospects," *J. Intell. Mater. Syst. Struct.*, vol. 17, no. 12, pp. 1041–1047, 2006.

[18] R. Noebe, T. Biles, and S. A. Padula, "NiTi-based high-temperature shape-memory alloys: properties, prospects, and potential applications," *Mater. Eng. YORK-*, vol. 32, p. 145, 2006.

[19] H. Sehitoglu *et al.*, "Superelasticity and shape memory behavior of NiTiHf alloys," *Shape Mem. Superelasticity*, vol. 3, pp. 168–187, 2017.

[20] Z. Xiao, Z. Li, M. Fang, S. Xiong, X. Sheng, and M. Zhou, "Effect of processing of mechanical alloying and powder metallurgy on microstructure and properties of Cu–Al–Ni–Mn alloy," *Mater. Sci. Eng. A*, vol. 488, no. 1–2, pp. 266–272, 2008.

_____

Engr. *Abid Hussain is currently pursuing PhD degree program in mechanical engineering department in University of Engineering and Technology peshawar, Pakistan,*

Prof. Dr. Afzal Khan *mechanical engineering department University of Engineering and Technology Peshawar, Pakistan,*

Dr. Muhammad Imran *Associate Prof. Ghulam Ishaq Khan (GIK) Institute of Engineering and Science and Technology, Topi District Swabi, Khyber Pakhtunkhawa 23640, Pakistan*

Dr. Saif Ur Rehman *Institute of Industrial Control System, Rawalpindi, Pakistan,*